

THE DETECTION OF OXYGEN IN THE LOW-DENSITY INTERGALACTIC MEDIUM¹

JOOP SCHAYE², MICHAEL RAUCH³, WALLACE L. W. SARGENT⁴, AND TAE-SUN KIM⁵

Accepted for publication in ApJ Letters

ABSTRACT

The abundances of metals in the intergalactic medium (IGM) can be used to constrain the amount of star formation at high redshift and the spectral shape of the ionizing background radiation. For both purposes it is essential to measure the abundances in regions of low density, away from local sources of metals and ionizing photons. Here we report the first detection of O VI in the low-density IGM at high redshift. We perform a pixel-by-pixel search for O VI absorption in eight high quality quasar spectra spanning the redshift range $z = 2.0$ - 4.5 . At $2 \lesssim z \lesssim 3$, we clearly detect O VI in the form of a positive correlation between the H I Ly α optical depth and the optical depth in the corresponding O VI pixel, down to $\tau_{\text{HI}} \sim 10^{-1}$. This is an order of magnitude lower in τ_{HI} than the best C IV measurements can probe and constitutes the first clear detection of metals in *underdense* gas. The non-detection of O VI at $z > 3$ is consistent with the enhanced photoionization from a hardening of the UV background below $z \sim 3$ but could also be caused by the high level of contamination from Ly series lines.

Subject headings: cosmology: observations — galaxies: formation — intergalactic medium — quasars: absorption lines

1. INTRODUCTION

The abundance of metals in the low-density intergalactic medium (IGM) at high redshift is of interest for at least two reasons. Firstly, the metallicity can be used to distinguish between different enrichment mechanisms and to constrain the amount of star formation at high redshift. Secondly, the relative abundances of ions with different ionization potentials can be used to derive the spectrum of the integrated UV background from stars and quasars. For both purposes it is essential to measure the metal abundances in gas of low density, away from the influence of local sources of ionizing radiation and locally produced metals.

Resonant Ly α absorption by neutral hydrogen along the line of sight to distant quasars results in a forest of absorption lines bluewards of the quasar's Ly α emission line. With the advent of the High-Resolution Echelle Spectrograph (HIRES) on the Keck telescope, it became clear that many of the high column density Ly α lines ($N_{\text{HI}} \gtrsim 10^{14.5} \text{ cm}^{-2}$) show associated C IV absorption (e.g., Cowie et al. 1995). Although increasing the signal-to-noise ratio (S/N) reveals C IV systems of progressively lower column density, C IV lines corresponding to low column density Ly α lines are generally far too weak to detect (e.g., Ellison et al. 2000).

The success of cosmological simulations in reproducing the observations of the Ly α forest has convincingly shown that the low column density forest ($N_{\text{HI}} \lesssim 10^{14.5} \text{ cm}^{-2}$) at high redshift ($z \gtrsim 2$) arises in a smoothly fluctuating IGM, with individual lines corresponding to local density maxima of moderate overdensity ($\rho/\bar{\rho} \lesssim 10$). The interplay between photoionization heating and adiabatic cooling that is due to the universal expansion results in a tight temperature-density relation, which is well approximated by a power-law, $T = T_0(\rho/\bar{\rho})^{\gamma-1}$ (Hui &

Gnedin 1997). The Ly α optical depth is proportional to the neutral hydrogen density, which in photoionization equilibrium is proportional to $\rho^2 T^{-0.76}$. Hence the optical depth depends on the underlying baryon overdensity, $\tau_{\text{HI}} \propto (\rho/\bar{\rho})^{2.76-0.76\gamma}$. The constant of proportionality is an increasing function of redshift, at $z \sim 3$, an optical depth of one corresponds to slightly overdense gas.

Cowie & Songaila (1998) realized that the tight correlation between optical depth and gas overdensity makes a pixel-by-pixel analysis of metal abundances useful. By measuring the median C IV/H I optical depth ratio as a function of τ_{HI} , they were able to show that the IGM is enriched with a roughly constant C IV/H I ratio down to $\tau_{\text{HI}} \sim 1$ at $z \sim 3$. Ellison et al. (2000) showed explicitly that directly detected C IV lines account for only a small fraction of the total amount of metals in the forest, as inferred from a pixel analysis.

Although other metal lines have been detected, C IV ($\lambda\lambda 1548, 1551$) has so far proven the most sensitive since it is the strongest line redwards of Ly α ($\lambda 1216$), where there is little contamination from other absorption lines. However, simulations show that at high redshift, photoionized O VI ($\lambda\lambda 1032, 1038$) should be a much better probe of the metallicity of the IGM in regions close to the mean density (Chaffee et al. 1986; Rauch, Haehnelt, & Steinmetz 1997; Hellsten et al. 1998). In practice it has proven very difficult to detect O VI at high redshift because it lies deep in the Ly α and Ly β ($\lambda 1026$) forest. Since Lu & Savage (1993) established the presence of O VI in intervening absorbers by stacking Lyman limit systems that show C IV absorption, O VI has been detected at high redshift in several Lyman limit systems (Vogel & Reimers 1995; Kirkman & Tytler 1997; 1999). Davé et al. (1998) (see also Cowie & Songaila 1998) carried out a thorough search for O VI but

¹Part of the data presented herein were obtained at the W. M. Keck Observatory, which is operated as a scientific partnership among the California Institute of Technology, the University of California and the National Aeronautics and Space Administration. The Observatory was made possible by the generous financial support of the W. M. Keck Foundation.

²Institute of Astronomy, Madingley Road, Cambridge CB3 0HA, UK; schaye@ast.cam.ac.uk

³Carnegie Observatories, 813 Santa Barbara Street, Pasadena, CA 91101; mr@ociw.edu

⁴Astronomy Department, California Institute of Technology, Pasadena, CA 91125; wws@astro.caltech.edu

⁵European Southern Observatory, Karl-Schwarzschild-Str. 2, 85748 Garching, Germany; tkim@eso.org

found only evidence for O VI associated with C IV absorption in high density gas.

At low redshift ($z \lesssim 1$), O VI absorbers have been shown to be common (e.g., Bergeron et al. 1994), so common in fact that they may harbor a large fraction of the baryons (Burles & Tytler 1996; Tripp, Savage & Jenkins 2000). These low redshift systems probably correspond to hot, shock heated gas in the potential wells of (groups of) galaxies, which may well be collisionally ionized.

We have carried out a pixel-by-pixel search for O VI in the spectra of eight quasars, spanning the redshift range $z \sim 2.0$ – 4.5 . We clearly detect O VI at $2 \lesssim z \lesssim 3$, down to very low H I optical depths, $\tau_{\text{HI}} \sim 10^{-1}$, which is an order of magnitude lower than the best C IV measurements can probe.

2. OBSERVATIONS AND SAMPLE DEFINITION

We analyzed spectra of the eight quasars listed in column 6 of Table 1. The spectra of Q1101, J2233 and Q1122 were taken during the Commissioning I and Science Verification observations of the UV-Visual Echelle Spectrograph (UVES) and have been released by ESO for public use. They were reduced with the ESO-maintained MIDAS ECHELLE package (see Kim, D’Odorico, & Cristiani 2000, in preparation) for details on the data reduction). The other spectra were obtained with the HIRES spectrograph (Vogt et al. 1994) on the Keck telescope. The reduction procedures for these quasars can be found in Barlow & Sargent (1997) and Sargent, Barlow & Rauch (2000, in preparation). The HIRES and UVES spectra have a nominal velocity resolution of 6.6 and 6.7 km s^{-1} (FWHM) and a pixel size of 0.04 and 0.05 \AA respectively. To avoid confusion with the $\text{Ly}\beta$ forest, we only used the $\text{Ly}\alpha$ region between the quasar’s $\text{Ly}\alpha$ and $\text{Ly}\beta$ emission lines. In addition, spectral regions close to the quasar (typically 5000 km s^{-1}) were excluded to avoid proximity effects. Regions in the $\text{Ly}\alpha$ forest thought to be contaminated by metal lines were excluded.

The mean absorption increases rapidly bluewards of the quasar’s $\text{Ly}\beta$ emission line because of the growing number of absorption lines other than $\text{Ly}\alpha$. For quasars at $z \gtrsim 3$ the increase in the absorption is dominated by higher order Ly lines, corresponding to $\text{Ly}\alpha$ lines which fall in between the quasar’s $\text{Ly}\beta$ and $\text{Ly}\alpha$ emission lines (i.e. in the $\text{Ly}\alpha$ forest). At lower redshift the hydrogen lines have smaller column densities and metal lines contribute significantly to the mean absorption. The increase in the mean absorption towards the blue, raises the threshold for detecting O VI absorption in the $\text{Ly}\alpha$ forest considerably. Moreover, the S/N in the O VI region generally decreases towards the blue, raising the detection threshold further. We therefore analyzed the red and blue halves, i.e. the high and low redshift halves, of each $\text{Ly}\alpha$ forest spectrum separately (for those quasars for which our spectral coverage extends far enough into the blue). This turned out to be crucial, as we were unable to detect O VI in any of the low redshift half samples. All the high redshift half samples are listed in Table 1.

⁶The spectrum is divided into chunks of 2 \AA and 250 spectra of length equal to the original spectrum are generated by picking chunks at random (with replacement, each chunk can be picked more than once). The 1σ error in the median is then the square root of the variance in the median over the bootstrap realizations.

TABLE 1
LIST OF SAMPLES

Sample	z_{min}	z_{max}	(S/N) _{OVI}	(S/N) _{HI}	QSO	z_{em}
1101	1.97	2.10	21	78	Q1101–264	2.14
2233	2.07	2.18	12	30	J2233–606	2.24
1122	2.03	2.34	27	66	Q1122–165	2.40
1442	2.51	2.63	8	61	Q1442+293	2.67
1107	2.71	2.95	10	49	Q1107+485	3.00
1425	2.92	3.14	42	113	Q1425+604	3.20
1422	3.22	3.53	46	105	Q1422+231	3.62
2237	4.15	4.43	31	32	Q2237–061	4.55

3. METHOD

We search for O VI using a variant of the pixel technique introduced by Cowie & Songaila (1998). We measure the optical depth in each $\text{Ly}\alpha$ forest pixel and in the corresponding O VI pixel. The H I–O VI pixel pairs are binned according to their H I optical depth and the median H I and O VI optical depths are computed for each bin. This technique enables us to probe the O VI abundance down to much lower densities than is possible by fitting lines. Its main advantage over, for example, the stacking method is its robustness. Being a median, it is relatively insensitive to (non-Gaussian) noise, contamination from non-O VI lines, problems that severely compromise the stacking method, which is a mean (see Ellison et al. 2000 for a critical assessment of both the stacking technique and the pixel technique for the case of C IV). Its main limitation is that it measures an *apparent* O VI optical depth, $\tau_{\text{OVI,app}}$, which is in general not the same as the true O VI optical depth because of contamination.

The effect of contaminating lines is reduced by defining $\tau_{\text{OVI,app}} \equiv \min(\tau_{\text{OVI,1032}}, 2\tau_{\text{OVI,1038}})$, where we used the fact that $(f\lambda)_{1032} = 2(f\lambda)_{1038}$. Taking the minimum doublet component does of course not guarantee that $\tau_{\text{OVI,app}} = \tau_{\text{OVI}}$. For some pixels both components may be contaminated, which would result in an overestimate of the O VI optical depth. However, if the contamination is negligible, then noise will cause us to underestimate τ_{OVI} . For C IV, which falls redwards of the $\text{Ly}\alpha$ forest, noise is the limiting factor and Ellison et al. (2000) therefore only used the weaker component if a 3σ detection was predicted, based on the signal in the stronger component. For O VI however, contamination is a much greater problem and we therefore take the the minimum if the expected signal in the weaker component is greater than 0.5σ , i.e. if $\exp(-0.5\tau_{\text{OVI,1032}}) < 1 - 0.5\sigma_{\text{OVI,1038}}$, where $\sigma_{\text{OVI,1038}}$ is the rms amplitude of the noise at the position of O VI, 1038 (as given by the normalized noise array).

When a pixel is close to saturation [$\exp(-\tau_{\text{HI}}) < 0.5\sigma$], we use up to 10 higher order Ly lines to determine the optical depth: $\tau_{\text{Ly}\alpha} \equiv \min(\tau_{\text{Ly}n} f_{\text{Ly}\alpha} \lambda_{\text{Ly}\alpha} / f_{\text{Ly}n} \lambda_{\text{Ly}n})$. We limit the effect of noise features by requiring $0.5\sigma_n < \exp(-\tau_{\text{Ly}n}) < 1 - 0.5\sigma_n$ (σ_n is the rms noise amplitude at the position of $\text{Ly}n$). The number of higher order lines available is different for each quasar spectrum and varies also within a single spectrum. However, since the number of pixels with a given τ_{HI} decreases rapidly for $\tau_{\text{HI}} \gtrsim 1$, the misbinning of H I due to missing higher orders affects only the highest τ_{HI} bins.

We use logarithmic τ_{HI} bins of size 0.35 dex (0.5 dex for the two lowest redshift quasars) and estimate the error in the medians by bootstrap resampling⁶.

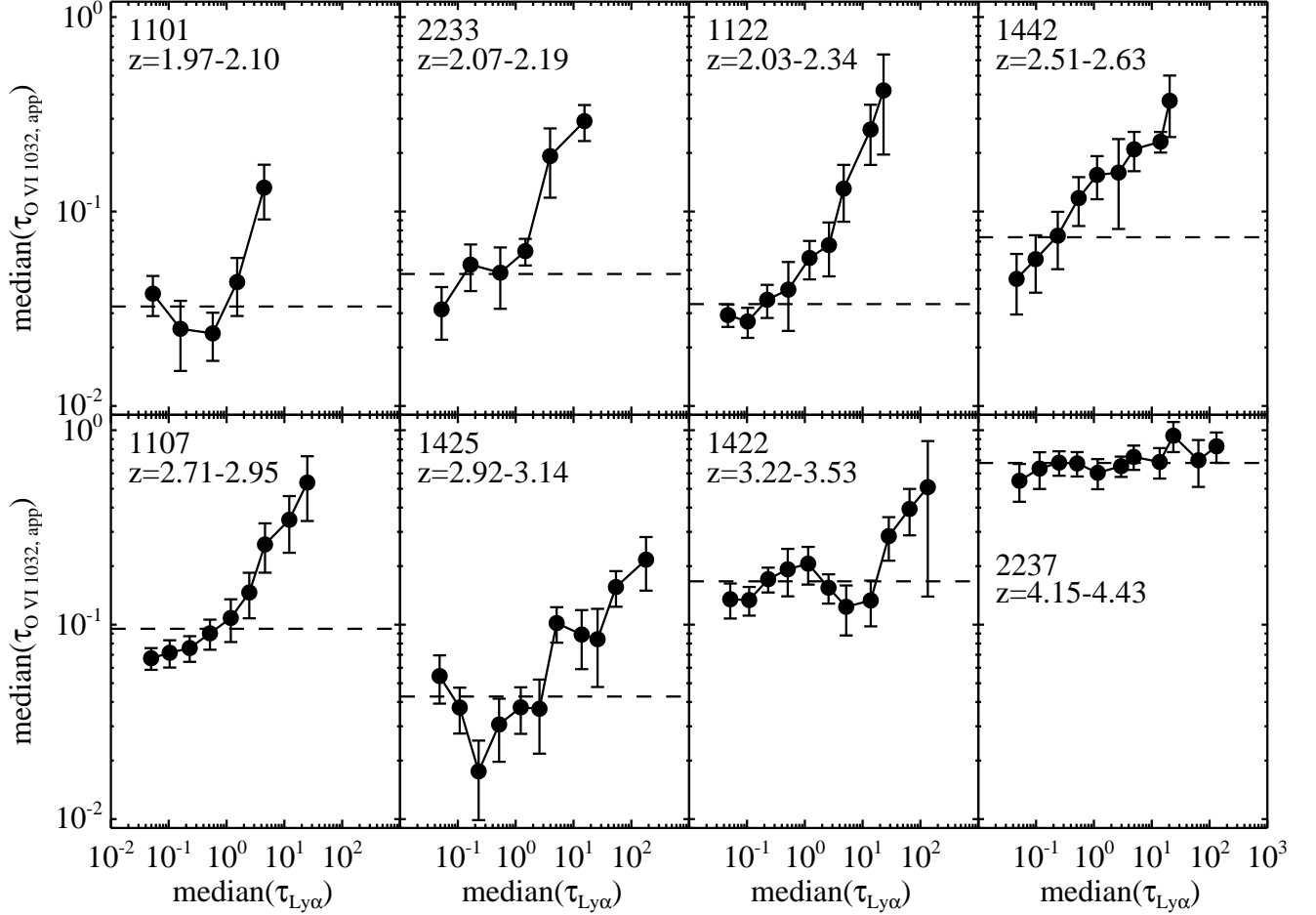


FIG. 1.— Results from the pixel analysis. For all HI Ly α pixels within the redshift range indicated in each panel, the corresponding OVI pixel was determined and the optical depths were measured. Pixels corresponding to higher order Ly lines and to the weaker line of the OVI doublet were used as described in section 3. HI-OVI pixel pairs were binned according to their HI optical depth and the data points indicate the median HI and OVI optical depth for each bin. The measured, apparent OVI optical depths include contributions from noise and contaminating non-OVI lines. The dashed lines show the median, apparent OVI optical depth for the full set of HI pixels. If the contribution of OVI to the median absorption is negligible, then the dashed lines are effectively the OVI detection limits. Vertical error bars are 1σ errors, horizontal error bars are smaller than the symbols and are not shown. For $z \lesssim 3$ $\tau_{\text{OVI,app}}$ and τ_{HI} are clearly correlated, down to optical depths as low as $\tau_{\text{HI}} \sim 10^{-1}$. A correlation between $\tau_{\text{OVI,app}}$ and τ_{HI} implies that OVI absorption has been detected in the Ly α forest.

4. RESULTS

Figure 1 shows the results from a pixel analysis of the samples listed in Table 1. The apparent OVI optical depth is clearly correlated with τ_{HI} at $z \lesssim 3$ down to $\tau_{\text{HI}} \sim 10^{-1}$, indicating that OVI is detected in the Ly α forest. At $z \sim 3.2$ – 3.5 we detect OVI only at very high HI optical depths, $\tau_{\text{HI}} > 10$, while at $z > 4$ τ_{OVI} and τ_{HI} appear uncorrelated. The transition seems to occur at $z \sim 3.0$ – 3.5 . If contamination and noise, which are independent of τ_{HI} , dominate over absorption from OVI, then $\tau_{\text{OVI,app}}$ will flatten off at the detection limit. Ellison et al. (2000) analyzed a very high quality spectrum of Q1422+231 ($(S/N)_{\text{CIV}} \sim 200$) and found that τ_{CIV} flattens off below $\tau_{\text{HI}} \sim 2$. We find that the correlation between $\tau_{\text{OVI,app}}$ and τ_{HI} continues down to much lower τ_{HI} , indicating that oxygen has been detected in gas of very low density contrast ($\rho/\bar{\rho} < 1$).

The horizontal, dashed lines indicate the median $\tau_{\text{OVI,app}}$ corresponding to a random HI pixel, i.e. the median $\tau_{\text{OVI,app}}$ for the set of all HI pixels. This reference level includes contributions from OVI, from contaminating non-OVI lines and from noise. For $z \gtrsim 3$, the contribution of OVI to this level is negligible

and the level is effectively the detection limit. For $z \lesssim 3$ on the other hand, OVI accounts for a significant part of the total absorption. Hence the detection limit is lower than the reference level and $\tau_{\text{OVI,app}}$ drops below the dashed line at low τ_{HI} .

We stress that because of noise and especially contamination, the measured, apparent OVI optical depths could differ considerably from the true values. We tried to estimate the effects of noise and contamination, which vary systematically across the spectrum, by analyzing synthetic spectra generated by drawing HI Voigt profiles at random from observed line lists until the mean absorption in the Ly α forest equals the observed value. We then added the corresponding OVI absorption lines using a fixed OVI/HI column density ratio and a fixed b -parameter ratio. Finally, higher order Ly lines and noise were added using the HI line list and the noise array respectively. We found that the simulations agree reasonably well with the observations for $N(\text{OVI})/N(\text{HI}) \sim 10^{-2}$ – 10^{-1} , although the results are sensitive to the assumed ratio of b -parameters. Although encouraging, these Monte Carlo simulations are clearly too simplistic to derive the intrinsic OVI/HI ratios. The effects of noise and contamination can only be modeled accurately by calibrating the

method against synthetic spectra extracted from hydrodynamic simulations. This should be done separately for each observed spectrum, using synthetic spectra that resemble the observed spectrum in detail. We leave such a quantitative analysis for a future paper but note that the effects that prevent us from deriving the actual O VI abundance, will reduce any intrinsic correlation between τ_{HI} and $\tau_{\text{OVI,app}}$, making a detection of such a correlation a robust result.

For a fixed O VI abundance, the value of the reference level (Fig. 1, dashed lines) increases with decreasing S/N and with increasing redshift. The latter effect is more important and is due to the increase in the number and strength of contaminating Ly series lines with redshift, which is a direct consequence of the expansion of the universe. As the universe expands, the column densities of lines corresponding to absorbers of a fixed overdensity decrease (the evolution of the ionizing background and the growth of structure are less important). This results in an increase of the amount of contamination, and thus the detection threshold, with redshift. Note that this effect is opposite to the increase in contamination towards the blue (i.e. low redshift) end of a single quasar spectrum, which is a consequence of the growing number of interlopers (see section 2). Like the column density, the H I optical depth corresponding to a fixed overdensity also increases with redshift. This complicates the comparison of the τ_{HI} level below which the correlation with O VI flattens off in samples of different redshifts. While an H I optical depth of one corresponds to about the mean density at $z \sim 3$, it corresponds to an overdensity of a few at $z \sim 2$ and to slightly underdense gas at $z \sim 4$.

For the quasars Q1107, Q1422 and Q2233 our spectral coverage is sufficient to analyze the blue half of the forest. We find no correlation between τ_{OVI} and τ_{HI} in any of these samples. As discussed above, this is a consequence of the large number of contaminating absorption lines from intervening absorbers and/or the low S/N of the data and does not imply that there is no O VI. In principle, even more O VI could be uncovered by looking at a smaller part of the spectrum. The contamination in the upper redshift quarter for example, will be lower than in the upper half. However, decreasing the number of pixels further would bring the redshift path into the regime of large-scale structures and the samples would therefore no longer be representative. This may already be the case for the two lowest redshift samples, for which the number of pixels showing H I absorption is much smaller than for the higher redshift samples. Nevertheless, we have tried smaller samples and found that the correlation strengthens somewhat for 1422 but not for 2237.

Figure 2 demonstrates that the O VI that we detect at low τ_{HI} is not associated with detectable C IV absorption. The solid line indicates the apparent O VI absorption in 1442. The dashed line shows the result obtained after all pixels that have nonzero C IV absorption at the 1σ level [$\exp(-\tau_{\text{CIV}}) < 1 - 1\sigma$] have been excluded. The dashed curve only falls below the solid curve for $\tau_{\text{HI}} \gtrsim 2$, indicating that some of the stronger O VI systems have been excluded. The fact that the two curves are almost indistinguishable for $\tau_{\text{HI}} \lesssim 2$ shows that O VI is detectable in absorbers for which C IV absorption is too weak to detect and is thus direct observational proof of the prediction that O VI is a more sensitive probe of the metallicity in low-density gas than C IV.

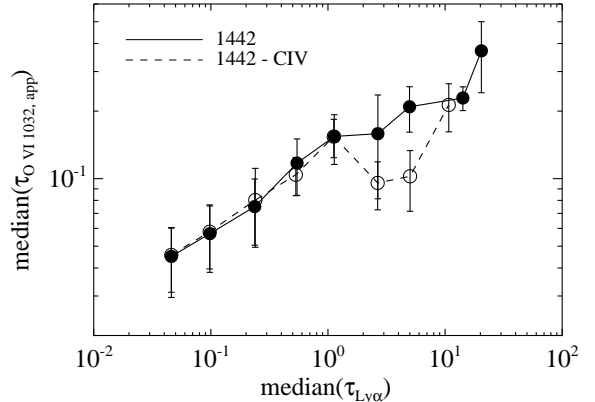


FIG. 2.— The effect of excluding CIV absorbers. The solid curve is for sample 1442. The dashed curve shows the result of the pixel analysis after having excluded all pixels for which the corresponding CIV absorption is detectable. The curves only start to differ at $\tau_{\text{HI}} \gtrsim 2$, indicating that only the strong OVI absorbers show significant CIV absorption.

5. DISCUSSION

We have searched for O VI absorption in the spectra of eight quasars spanning the redshift range $z \sim 2.0$ – 4.5 and reported the first detection of O VI in the low-density IGM at high redshift. We analyzed the spectra pixel by pixel and detected a positive correlation between the optical depths in H I and in the corresponding O VI pixels down to $\tau_{\text{HI}} \sim 10^{-1}$ at $2 \lesssim z \lesssim 3$. This is an order of magnitude lower in τ_{HI} than the best C IV measurements can probe and constitutes the first firm detection of metals in *underdense* gas. We showed that the O VI signal does not come from systems for which C IV is detectable, and this confirms the prediction that O VI is a much better tracer of metals in low-density gas than C IV.

Although the very strong absorbers may well be collisionally ionized (e.g., Kirkman & Tytler 1999), the volume filling factor of this hot gas is much smaller than that of photoionized gas (e.g., Cen & Ostriker 1999). The ubiquitous O VI detected here, arises in gas that is too dilute for collisional ionization to be effective. Photons of at least 8.4 Ryd are needed to create O VI and hence we would not expect to detect photoionized O VI if the reionization of He II, for which photons of at least 4 Ryd are required, is not yet complete. Measurements of the He II Ly α opacity (Heap et al. 2000 and references therein) and the temperature of the IGM (Schaye et al. 2000, Ricotti, Gnedin & Shull 2000) suggest that the reionization of helium may have been completed at $z \sim 3$. Although our non-detection of O VI at $z > 3$ is consistent with enhanced photoionization from a hardening of the ionizing background below $z \sim 3$, it could also be caused by the increased level of contamination from Ly series lines.

Our detection of O VI down to $\tau_{\text{HI}} \sim 10^{-1}$ shows that the IGM is enriched down to much lower overdensities than have been probed up till now. A comparison with simulations could clarify how noise and contamination from Ly series lines affect the apparent O VI optical depth, what fraction of the low-density gas is enriched and what the scatter in the O VI/H I ratio is, thereby providing strong constraints on theoretical models for the enrichment of the IGM.

We are grateful to S. Ellison, M. Pettini and G. Efstathiou for discussions and a careful reading of the manuscript. JS thanks the Isaac Newton Trust and PPARC for support. WLWS acknowledges support from the NSF under grant AST-9900733.

REFERENCES

- Barlow, T. A., & Sargent, W. L. W. 1997, *AJ*, 113, 136
Bergeron, J., et al. 1994, *ApJ*, 436, 33
Burles, S., & Tytler, D. 1996, *ApJ*, 460, 584
Cen, R., & Ostriker, J. P. 1999, *ApJ*, 514, 1
Chaffee, F. H., Foltz, C. B., Bechthold, J., & Weymann, R. J. 1986, *ApJ*, 301, 116
Cowie, L. L., & Songaila, A. 1998, *Nature*, 394, 44
Cowie, L. L., Songaila, A., Kim, T.-S., & Hu, E. M. 1995, *AJ*, 109, 1522
Davé, R., Hellsten, U., Hernquist, L., Katz, N., & Weinberg, D. H. 1998, *ApJ*, 509, 661
Ellison, S. L., Songaila, A., Schaye, J., & Pettini, M. 2000, *AJ*, in press (astro-ph/0005448)
Heap, S. R., Williger, G. M., Smette, A., Hubeny, I., Sahu, M., Jenkins, E. B., Tripp, T. M., & Winkler, J. N. 2000, *ApJ*, 534, 69
Hellsten, U., Hernquist, L., Katz, N., & Weinberg, D. H. 1998, *ApJ*, 499, 172
Hui, L., & Gnedin, N. Y. 1997, *MNRAS*, 292, 27
Kirkman, D., & Tytler, D. 1997, *ApJ*, 489, L123
Kirkman, D., & Tytler, D. 1999, *ApJ*, 512, L5
Lu, L., & Savage, B. D. 1993, *ApJ*, 403, 127
Rauch, M., Haehnelt, M. G., & Steinmetz, M. 1997, *ApJ*, 481, 601
Ricotti, M., Gnedin, N. Y., & Shull, J. M. 2000, *ApJ*, 534, 41
Schaye, J., Theuns, T., Rauch, M., Efstathiou, G., & Sargent, W. L. W. 2000, *MNRAS*, in press (astro-ph/9912432)
Tripp, T. M., Savage, B. D., & Jenkins, E. B. 2000, *ApJ*, 534, L1
Vogel, S., & Reimers, D. 1995, *A&A*, 294, 377
Vogt, S. S., et al. 1994, *Proc. Soc. Photo-Opt. Instrum. Eng.*, 2198, 362